Journal of Molecular Spectroscopy **196,** 120–130 (1999)
Article ID jmsp.1999.7844, available online at http://www.idealibrary.com on IDEAL®

Infrared Spectroscopy of H_3O^+: The ν_1 Fundamental Band

Jian Tang and Takeshi Oka

Department of Chemistry, Department of Astronomy and Astrophysics, The Enrico Fermi Institute, The University of Chicago, Illinois 60637

E-mail: t-oka@uchicago.edu

Received December 24, 1998

The infrared spectrum of H_3O^+ in positive column discharges of H_2/O_2 gas mixtures has been studied by a difference frequency laser spectrometer. The ν_1 fundamental band of H_3O^+ was identified in the region of the strong $\nu_3^{\pm} \leftarrow 0^{\pm}$ bands. Molecular constants were obtained by the least-squares fitting of the observed frequencies, and band origins of the $\nu_1^+ \leftarrow 0^-$ and $\nu_1^- \leftarrow 0^+$ subbands were determined to be 3389.656(2) and 3491.170(2) cm^{-1}, respectively. During this study, assignment of the ν_3 fundamental band was extended to higher J, K transitions, which do not fit to the calculated pattern well, but have definitely been assigned by using the ground state combination differences and relative intensities. Vibration–rotation interactions between the ν_1 and ν_3 states have been considered, which explained some large discrepancies between observed and calculated frequencies and led to the identification of forbidden transitions. Energy differences in the ground state between the $\Delta K = 3$ rotational levels were obtained from the combination differences of the forbidden and allowed transitions, which led to an accurate determination of C and D_K. Equilibrium structure of H_3O^+ has been derived to be $r_e = 0.974(1)$ Å and $\alpha_e = 113.6(1)°$.

Key Words: infrared spectroscopy; H_3O^+; vibration–inversion–rotation

1. INTRODUCTION

The hydronium ion H_3O^+, or the protonated water, is a fundamental species in both terrestrial chemical processes and interstellar chemistry. The first high-resolution spectrum of H_3O^+ was reported in 1983 for the infrared ν_3 fundamental band without assignment (*1*), and this was followed by more detailed studies of the same band (*2–6*). The vibration–inversion–rotation spectrum of the ν_2 band of this NH_3-like species was studied extensively from 10 to 30 μm (*7–14*) and led to the determination of the inversion splitting of H_3O^+ (*12*). The ν_4 fundamental band (*15*) and the $\nu_2 + \nu_3 \leftarrow \nu_2$ hot band (*5*) have also been studied. Based on the observed inversion splitting, 55.35 cm^{-1} (*12*), which is much larger than that of the isoelectronic NH_3, 0.79 cm^{-1}, rotation–inversion (*16–18*) and pure inversion (*19*) spectra of H_3O^+ were observed in the submillimeter-wave and far-infrared region, respectively. The laboratory submillimeter-wave spectrum has led to the initially somewhat uncertain (*20, 21*) but later more convincing (*22, 23*) detection of interstellar H_3O^+. A possible astronomical detection of a far-infrared line has recently been reported (*24*). As a key molecular ion for the oxygen chemistry, the observed interstellar abundance of H_3O^+ has been used to estimate the interstellar abundance of O_2 and H_2O which are very important but difficult to determine directly (*23*). These developments have provided nearly complete information on intramolecular dynamics of H_3O^+ except for the totally symmetric OH stretching ν_1 band. Apart from a strong and broad Raman band observed in solution and assigned to the ν_1 band by Giguère and Madec (*25*), there has previously been no report on this band. In this paper, we report our observation and analysis of this band.

Because of the importance of H_3O^+ both in chemistry and molecular astrophysics, extensive theoretical studies have been reported on the potential surface, geometric structure, and spectroscopic properties of H_3O^+ (*26–35*). Accurate calculation of the large inversion frequency in H_3O^+ has been a challenge for theorists, and this has not been achieved satisfactorily even today. Although the observed vibration–inversion frequencies for the ν_2, ν_3, and ν_4 fundamental bands were used for determining the potential surface by Špirko and Kraemer (*33*), their calculated vibration–inversion frequencies for the ν_1 fundamental band were far from observed. It is our hope that the new experimental information on the ν_1 vibration can help theorists to improve the potential surface of H_3O^+.

Ab initio calculations have given different predictions for the vibrational frequency and the inversion splitting in the ν_1 state, 3546 and 38 (*30*), 3570 and 68 (*33*), and 3437 cm^{-1} without considering inversion (*34*). The infrared intensity ratios for the four fundamental ν_1, ν_2, ν_3, and ν_4 bands of H_3O^+ were calculated (*29, 34*) to be about 1:11:12:3. Botschwina *et al.* (*30*) calculated infrared intensities for symmetric vibrations and gave the ratios for the bands of $\nu_1^- \leftarrow 0^+$, $\nu_1^+ \leftarrow 0^-$, $\nu_2^- \leftarrow 0^+$, and $\nu_2^+ \leftarrow 0^-$ (superscript + or − represents the parity of inversion state) as 1:1:30:120, in which the intensity ratio of $\nu_2^- \leftarrow 0^+$ to $\nu_2^+ \leftarrow 0^-$ was in very good agreement with the observed value (*11*). Because the ν_1 band appears in the same region as the ν_3 band and is about 10 times weaker than the ν_3 band, the identification of the ν_1 band was not straightforward, especially in view of the fact that ν_3 transitions involving higher J, K quantum states had not been assigned.

Our previous infrared spectrum of H_3O^+ had been recorded by a color-center (*5*) and a difference-frequency laser spectrometer

0022-2852/99 $30.00

TABLE 1

Newly Assigned Transitions of the ν_3 Fundamental Band of H_3O^+ (in cm^{-1})

J' K' l' J K	Obs.	O-C	J' K' l' J K	Obs.	O-C	J' K' l' J K	Obs.	O-C
$\nu_3^+ \leftarrow 0^+$								
10 7 1 11 6	3207.527	-0.853[a]	12 10 -1 13 11	3347.941	-2.129[a]	7 7 1 7 6	3460.758	-0.131[a]
9 8 1 10 7	3223.303	-0.382[a]	5 5 1 6 4	3349.317	-0.154[a]	8 6 1 8 5	3466.234	-0.423[a]
9 7 1 10 6	3232.351	-0.534[a]	13 12 -1 14 13	3351.654	-1.418[a]	7 6 1 7 5	3469.473	-0.230[a]
8 8 1 9 7	3248.068	-0.146[a]	6 2 1 7 1	3354.648	0.032[a]	6 6 1 6 5	3472.298	-0.110[a]
8 7 1 9 6	3257.154	-0.276[a]	14 14 -1 15 15	3356.882	-0.002	7 5 1 7 4	3479.965	1.245[a,b]
9 2 1 10 1	3280.274	-0.071[a]	10 7 -1 11 8	3357.931	-2.436[a]	6 5 1 6 4	3481.023	-0.469[a]
7 7 1 8 6	3281.837	-0.120[a]	11 9 -1 12 10	3360.369	-1.672[a]	5 5 1 5 4	3483.749	-0.154[a,b]
8 4 1 9 3	3285.597	-0.005	12 11 -1 13 12	3363.621	-1.138[a]	8 4 1 8 3	3484.808	0.013[b]
7 6 1 8 5	3291.021	-0.223[a]	6 1 1 7 0	3363.940	0.090[a]	7 4 1 7 3	3487.936	-0.053[a]
8 3 1 9 2	3295.262	-0.054[a]	9 6 -1 10 7	3367.969	-4.821[a]	8 3 1 8 2	3494.218	-0.050[a]
9 0 -1 10 1	3301.694	-0.069[a]	13 13 -1 14 14	3368.380	0.001	10 2 1 10 1	3496.111	-0.007
7 5 1 8 4	3301.908	1.260[a]	10 8 -1 11 9	3372.654	-1.439[a]	9 2 1 9 1	3500.221	-0.023
8 2 1 9 1	3305.156	-0.052[a]	8 4 -1 9 5	3372.726	0.070[a]	9 1 1 9 0	3513.136	-0.292[a]
14 11 -1 15 12	3307.847	-3.927[a]	11 10 -1 12 11	3375.579	-0.921[a]	9 0 -1 9 1	3521.730	0.063[a]
10 3 -1 11 4	3310.159	0.106[a]	12 12 -1 13 13	3379.893	-0.002	8 0 -1 8 1	3525.382	0.031[a]
7 4 1 8 3	3310.201	-0.016	9 7 -1 10 8	3384.835	-1.384[a]	9 1 -1 9 2	3532.618	0.087[a]
9 1 -1 10 2	3312.434	-0.033[a]	10 9 -1 11 10	3387.536	-0.754[a]	8 1 -1 8 2	3536.382	0.026[a]
8 1 1 9 0	3313.442	-0.125[a]	8 6 -1 9 7	3395.100	-3.309[a]	9 3 -1 9 4	3556.100	0.115[a]
6 6 1 7 5	3315.605	-0.103[a]	9 8 -1 10 9	3399.506	-0.619[a]	8 4 -1 8 5	3572.729	0.106[a]
7 3 1 8 2	3319.961	-0.031[a,b]	8 7 -1 9 8	3411.383	-0.616[a]	7 4 -1 7 5	3576.357	0.018
6 5 1 7 4	3324.687	-0.443[a]	7 6 -1 8 7	3422.740	-1.167[a]	9 6 -1 9 7	3590.440	-4.831[a]
8 0 -1 9 1	3326.516	-0.028[a]	10 8 1 10 7	3441.910	-0.818[a]	5 5 1 4 4	3596.081	-0.136[a]
15 14 -1 16 15	3327.844	-2.033[a]	9 8 1 9 7	3445.780	-0.386[a]	8 6 -1 8 7	3596.187	-3.349[a,b]
12 9 -1 13 10	3333.014	-2.815[a]	11 7 1 11 6	3446.072	-1.283[a]	7 6 -1 7 7	3602.322	-1.077[a]
9 3 -1 10 4	3335.330	0.054[a]	6 6 -1 7 7	3448.476	-0.752[a]	6 5 1 5 4	3615.465	-0.459[a]
13 11 -1 14 12	3335.625	-2.563[a]	8 8 1 8 7	3449.198	-0.142[a]	9 8 -1 9 9	3623.640	-0.685[a]
8 1 -1 9 2	3337.399	-0.005	10 7 1 10 6	3450.291	-0.844[a]	7 5 1 6 4	3636.320	1.238[a]
14 13 -1 15 14	3339.736	-1.708[a]	9 7 1 9 6	3454.136	-0.532[a]	10 9 -1 10 10	3634.100	-0.725[a]
11 8 -1 12 9	3345.525	-2.518[a,b]	8 7 1 8 6	3457.635	-0.293[a]			
$\nu_3^- \leftarrow 0^-$								
9 7 1 10 6	3223.587	0.000	11 8 -1 12 9	3331.492	-1.822[a]	6 6 -1 7 7	3431.290	-0.312[a]
10 3 1 11 2	3237.144	-0.101[a]	12 10 -1 13 11	3332.208	-1.275[a]	9 4 1 9 3	3470.009	0.300[a]
9 5 1 10 4	3242.166	-0.022[a]	9 4 -1 10 5	3335.548	0.516[a]	7 4 1 7 3	3474.543	-0.039[a]
8 7 1 9 6	3247.505	0.006	14 14 -1 15 15	3335.722	0.127[a]	9 2 1 9 1	3488.116	0.010
9 4 1 10 3	3251.612	-0.054[a]	8 2 -1 9 3	3337.641	0.176[a]	10 0 -1 10 1	3505.933	0.112[a]
8 6 1 9 5	3256.779	0.033[a]	10 7 -1 11 8	3343.924	-1.923[a]	9 0 -1 9 1	3509.011	0.038[a]
9 3 1 10 2	3261.219	-0.056[a]	11 9 -1 12 10	3344.720	-1.108[a]	9 2 -1 9 3	3529.688	0.194[a,b]
8 5 1 9 4	3266.134	0.023[a]	12 11 -1 13 12	3345.720	-0.746[a]	6 2 -1 6 3	3538.740	-0.033[a,b]
10 0 -1 11 1	3267.985	0.100[a]	13 13 -1 14 14	3347.551	-0.143[a]	9 3 -1 9 4	3541.718	0.238[a]
9 2 1 10 1	3270.942	-0.021	9 5 -1 10 6	3347.704	1.137[a]	8 3 -1 8 4	3544.720	0.100[a]
7 7 1 8 6	3271.359	-0.001	8 3 -1 9 4	3348.113	0.097[a]	7 3 -1 7 4	3547.496	0.038[a,b]
8 4 1 9 3	3275.784	0.172[a]	9 6 -1 10 7	3354.712	-3.692[a]	8 4 -1 8 5	3556.483	0.234[a]
9 1 1 10 0	3278.829	0.008	10 8 -1 11 9	3357.138	-1.048[a]	7 4 -1 7 5	3559.240	0.103[a]
7 6 1 8 5	3280.620	0.018	11 10 -1 12 11	3358.051	-0.607[a]	10 5 -1 10 6	3562.879	1.440[a]
7 5 1 8 4	3289.999	0.029[a]	8 4 -1 9 5	3359.604	0.255[a]	9 5 -1 9 6	3566.104	1.113[a]
9 0 -1 10 1	3291.837	0.006	12 12 -1 13 13	3359.767	0.002	9 6 -1 9 7	3573.615	-3.689[a]
14 11 -1 15 12	3292.957	-2.971[a]	7 2 -1 8 3	3360.780	0.037[a]	8 6 -1 8 7	3578.302	-2.314[a]
8 2 1 9 1	3295.025	-0.009	9 7 -1 10 8	3369.487	-1.066[a]	11 7 -1 11 8	3579.535	-2.812[a]
7 4 1 8 3	3299.493	0.006	10 9 -1 11 10	3370.334	-0.510[a]	7 6 -1 7 7	3582.439	-1.165[a]
12 8 -1 13 9	3305.625	-2.827[a]	11 11 -1 12 12	3371.818	0.008	10 7 -1 10 8	3584.397	-1.924[a]
13 10 -1 14 11	3306.168	-2.182[a]	7 3 -1 8 4	3372.164	0.007	12 8 -1 12 9	3588.138	-2.834[a]
9 2 -1 10 3	3312.251	0.192[a]	8 6 -1 9 7	3380.601	-2.324[a]	9 7 -1 9 8	3589.080	-0.922[a,b]
11 7 -1 12 8	3318.267	-2.844[a]	9 8 -1 10 9	3382.579	-0.442[a]	8 7 -1 8 8	3592.933	-0.439[a]
12 9 -1 13 10	3319.010	-1.804[a,b]	7 4 -1 8 5	3383.688	0.115[a]	11 8 -1 11 9	3593.454	-1.843[a]
13 11 -1 14 12	3319.594	-1.561[a]	6 2 -1 7 3	3385.077	-0.070[a]	10 8 -1 10 9	3598.290	-1.055[a]
10 5 -1 11 6	3323.520	1.427[a]	8 7 -1 9 8	3394.731	-0.455[a]	9 8 -1 9 9	3602.646	-0.447[a]
15 15 -1 16 16	3323.840	0.370[a,b]	7 6 -1 8 7	3406.174	-1.163[a]	12 11 -1 12 12	3631.250	-0.735[a]
9 3 -1 10 4	3324.023	0.234[a]	6 5 -1 7 6	3419.666	0.196[a]	9 1 1 8 0	3692.076	0.073[a]

[a] Transitions not used in the fitting.

[b] Overlapped lines.

(*6*). Since the target species for these sweeps was another molecular ion, HO_2^+, the discharge gases were either H_2/O_2/He mixture or H_2O_2/He mixture and the ions were produced predominantly by Penning ionization. This yielded extremely rich spectral lines. Finding the weak ν_1 band was not easy. In the present study, we optimized the plasma chemical condition for generating the H_3O^+

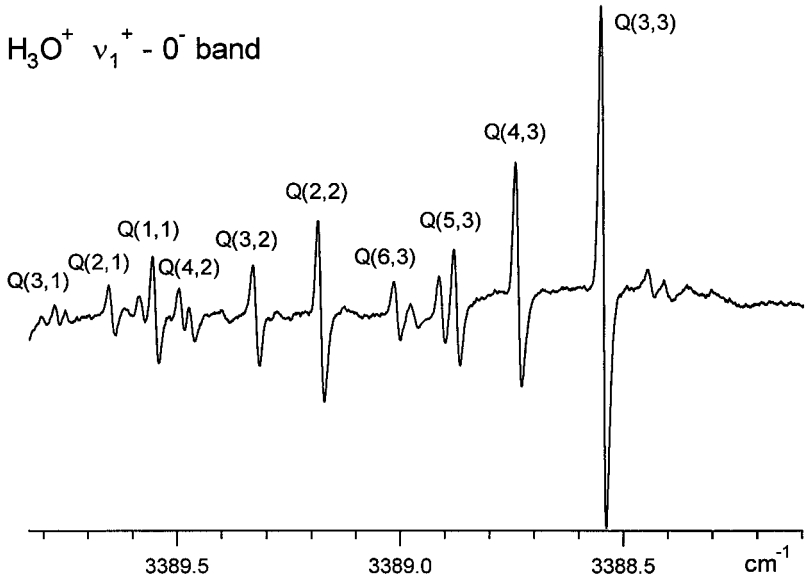

FIG. 1. A portion of the observed spectrum for the Q branch of the $\nu_1^+ \leftarrow 0^-$ band. Conditions of the glow discharge were a current of 130 mA and a frequency of 7 kHz for a gas mixture of H_2/O_2 = 1.8/0.3 Torr. The scan was taken with a speed of 1 cm^{-1} per 10 min with the detection time constant of 3 s. The first-derivative lineshape is due to the velocity modulation.

molecular ion and obtained a remarkably simpler spectrum. After extending the previous assignment (*5*) of the ν_3 band to higher J, K transitions, the vibration–inversion–rotation structure of the ν_1 fundamental band was finally identified.

II. EXPERIMENTAL

A difference-frequency laser spectrometer (*36, 37*) was used to scan in the 3-μm infrared region. Briefly, continuously tunable infrared radiation (~200 μW) was generated from a $LiNbO_3$ crystal, through which two orthogonally polarized visible beams from an Ar^+ laser (~1 W) and a tunable ring dye laser (~1 W) passed collinearly. The infrared radiation was divided into two beams with equal energy, and the two beams was traversed through the plasma in opposite directions with each beam multireflected four times in unidirection. By using the velocity modulation (*38*), the two beams carried signals in opposite phases but noise in the same phase, and subtracting the two detected signals allowed us to conduct highly sensitive spectroscopy, which picks up only ion signals.

The H_3O^+ ion was generated by an AC glow discharge of

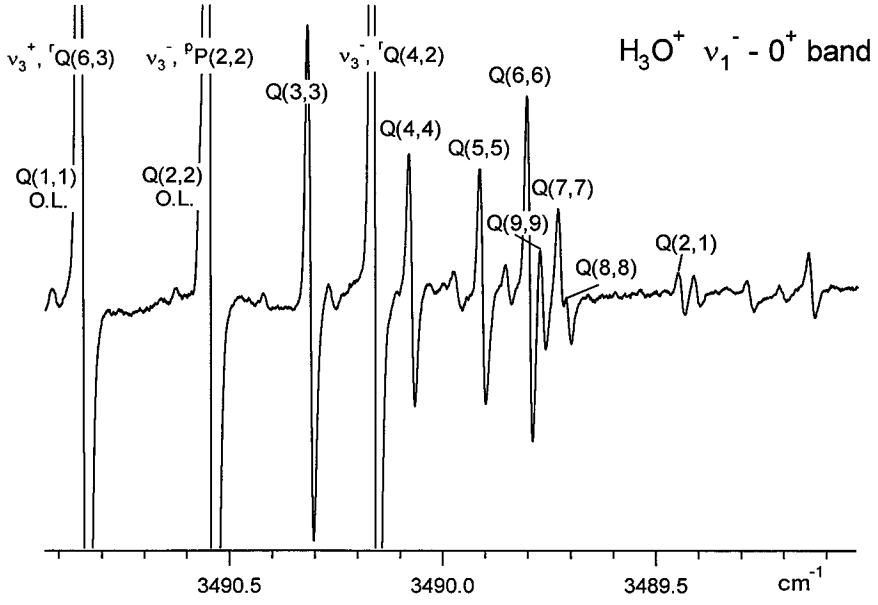

FIG. 2. A portion of the observed spectrum for the Q branch of the $\nu_1^- \leftarrow 0^+$ band. The transitions $Q(1, 1)$ and $Q(2, 2)$ were overlapped with strong transitions of the ν_3 fundamental band. Experimental conditions were the same as in Fig. 1.

TABLE 2
Observed Transitions of the ν_1 Fundamental Band of H_3O^+ (in cm^{-1})

J' K' J K	Obs.	O-C	J' K' J K	Obs.	O-C	J' K' J K	Obs.	O-C
$\nu_1^- \leftarrow 0^+$								
7 4 8 4	3299.684	-0.004	3 3 4 3	3400.416	-0.001[b]	5 5 5 5	3489.927	-0.001
6 0 7 0	3321.361	0.049[a]	2 0 3 0	3421.716	0.001	4 4 4 4	3490.092	-0.004
6 1 7 1	3321.599	-0.001	2 1 3 1	3422.061	0.000	3 3 3 3	3490.304	-0.002
6 2 7 2	3322.451	-0.022[a]	2 2 3 2	3423.135	0.026[a,b]	2 2 2 2	3490.566	0.011[a,b]
6 3 7 3	3323.840	-0.120[a,b]	1 1 2 1	3445.860	0.001	1 1 1 1	3490.827	-0.016[a,b]
6 4 7 4	3326.232	0.121[a,b]	6 3 6 3	3479.965	-0.094[a,b]	2 0 1 0	3534.071	0.002
6 5 7 5	3329.101	0.108[a]	6 4 6 4	3482.582	0.109[a]	2 1 1 1	3534.438	-0.004
6 6 7 6	3332.698	0.005	5 3 5 3	3484.057	-0.041[a,b]	3 1 2 1	3554.793	-0.003
5 1 6 1	3347.391	0.001	7 6 7 6	3484.808	0.001[b]	3 2 2 2	3555.927	0.004
5 2 6 2	3348.387	0.071[a]	6 5 6 5	3485.821	0.128[a]	4 0 3 0	3574.035	0.004
5 3 6 3	3349.854	-0.038[a]	5 4 5 4	3486.771	0.173[a]	4 1 3 1	3574.397	-0.004
5 4 6 4	3352.335	0.169[a]	3 1 3 1	3487.403	-0.011[a,b]	4 2 3 2	3575.510	-0.003
5 5 6 5	3355.200	-0.007[b]	4 3 4 3	3487.523	-0.002	4 3 3 3	3577.414	0.000
4 0 5 0	3372.450	-0.001	3 2 3 2	3488.480	0.003[b]	5 2 4 2	3594.430	0.077[a]
4 1 5 1	3372.775	0.003	2 1 2 1	3489.462	0.004	5 3 4 3	3596.187	-0.037[a,b]
4 2 5 2	3373.749	0.004	8 8 8 8	3489.720	-0.003	5 4 4 4	3599.078	0.166[a]
4 3 5 3	3375.394	-0.005	7 7 7 7	3489.737	0.001	6 0 5 0	3611.030	0.023[a]
4 4 5 4	3377.784	0.002	9 9 9 9	3489.777	0.001	6 1 5 1	3611.310	-0.036[a]
3 1 4 1	3397.681	-0.001	6 6 6 6	3489.807	0.001	6 3 5 3	3614.110	-0.155[a]
3 2 4 2	3398.695	0.000	10 10 10 10	3489.865	-0.041[a]	6 4 5 4	3617.060	0.155[a]
$\nu_1^+ \leftarrow 0^-$								
8 8 9 8	3183.182	0.070[a]	2 2 3 2	3322.910	-0.004	3 1 3 1	3389.775	-0.004
8 7 9 7	3186.102	0.038[a]	2 1 3 1	3323.420	0.000	4 1 4 1	3389.905	-0.005
8 6 9 6	3189.556	1.174[a]	1 1 2 1	3345.358	0.001	5 1 5 1	3390.010	0.002[b]
7 7 8 7	3207.032	0.004	1 0 2 0	3345.525	0.002[b]	6 1 6 1	3390.010	-0.020[a,b]
7 6 8 6	3209.499	-0.005	9 9 9 9	3378.894	-0.121[a]	1 0 0 0	3411.811	-0.003
7 5 8 5	3211.591	0.166[a]	8 8 8 8	3381.367	0.070[a]	2 1 1 1	3433.846	0.003
7 4 8 4	3213.669	0.791[a,b]	9 8 9 8	3381.529	-0.329[a]	3 2 2 2	3455.588	0.001
7 3 8 3	3213.669	-0.265[a,b]	7 7 7 7	3383.292	-0.003	3 1 2 1	3456.011	0.002
7 2 8 2	3214.579	-0.070[a]	8 7 8 7	3383.792	0.037[a]	3 0 2 0	3456.148	0.001
7 1 8 1	3215.062	0.000	6 6 6 6	3385.013	-0.002	4 3 3 3	3477.044	-0.001
7 0 8 0	3215.230	0.033[a]	7 6 7 6	3385.389	-0.001	4 2 3 2	3477.720	0.003
6 6 7 6	3230.703	0.007	5 5 5 5	3386.456	-0.003	4 1 3 1	3478.110	0.005
6 5 7 5	3232.733	0.005	6 5 6 5	3386.767	0.002	5 4 4 4	3498.216	-0.003
6 4 7 4	3235.114	0.842[a]	8 6 8 6	3386.881	1.236[a]	5 3 4 3	3499.087	-0.034[a]
6 3 7 3	3235.238	-0.162[a]	7 5 7 5	3387.157	0.168[a,b]	5 2 4 2	3499.700	-0.026[a]
6 2 7 2	3236.118	-0.047[a]	4 4 4 4	3387.632	-0.001	5 1 4 1	3500.059	-0.014[a,b]
6 1 7 1	3236.602	-0.007	5 4 5 4	3387.877	-0.002	5 0 4 0	3500.182	-0.004
5 5 6 5	3254.109	-0.008	3 3 3 3	3388.542	0.003	6 5 5 5	3519.114	0.007
5 4 6 4	3255.730	-0.005	4 3 4 3	3388.735	0.002[b]	6 3 5 3	3520.887	-0.130[a]
5 3 6 3	3256.884	-0.035[a]	7 3 7 3	3388.735	-0.294[a,b]	6 4 5 4	3521.046	0.823[a,b]
5 2 6 2	3257.708	-0.018[a]	5 3 5 3	3388.877	-0.033[a,b]	6 2 5 2	3521.488	-0.056[a]
5 1 6 1	3258.186	-0.008	6 3 6 3	3388.877	-0.149[a,b]	6 1 5 1	3521.832	-0.013[a]
5 0 6 0	3258.356	0.009	6 4 6 4	3388.908	0.830[a]	7 6 6 6	3539.710	0.001
4 4 5 4	3277.299	0.005	7 4 7 4	3388.970	0.792[a]	7 5 6 5	3541.185	0.160[a]
4 3 5 3	3278.525	0.003	2 2 2 2	3389.177	0.000	7 3 6 3	3542.383	-0.273[a]
4 2 5 2	3279.359	0.000	3 2 3 2	3389.326	0.002	7 4 6 4	3542.731	0.747[a]
4 1 5 1	3279.850	0.005	4 2 4 2	3389.490	0.012[a]	7 2 6 2	3543.021	-0.075[a]
3 3 4 3	3300.225	-0.001	1 1 1 1	3389.551	0.001	7 1 6 1	3543.347	0.003
3 2 4 2	3301.084	-0.001	5 2 5 2	3389.584	-0.022[a]	7 0 6 0	3543.464	0.040[a,b]
3 1 4 1	3301.583	-0.001	6 2 6 2	3389.614	-0.049[a]	8 6 7 6	3562.738	1.207[a]
3 0 4 0	3301.747	-0.001	2 1 2 1	3389.646	-0.004			

[a] Transitions not used in the fitting.

[b] Overlapped lines.

H_2/O_2 gas mixtures in a liquid-nitrogen-cooled multiple inlet–outlet glass cell (nicknamed "black widow") with 1-m length and 12-mm inner diameter. The optimum condition had a pressure of 1.8 Torr H_2 and 0.3 Torr O_2, a discharge current of 130 mA, and a discharge frequency of 7 kHz. In this H_2-dominant positive column discharge, the spectrum was much simpler than previ-

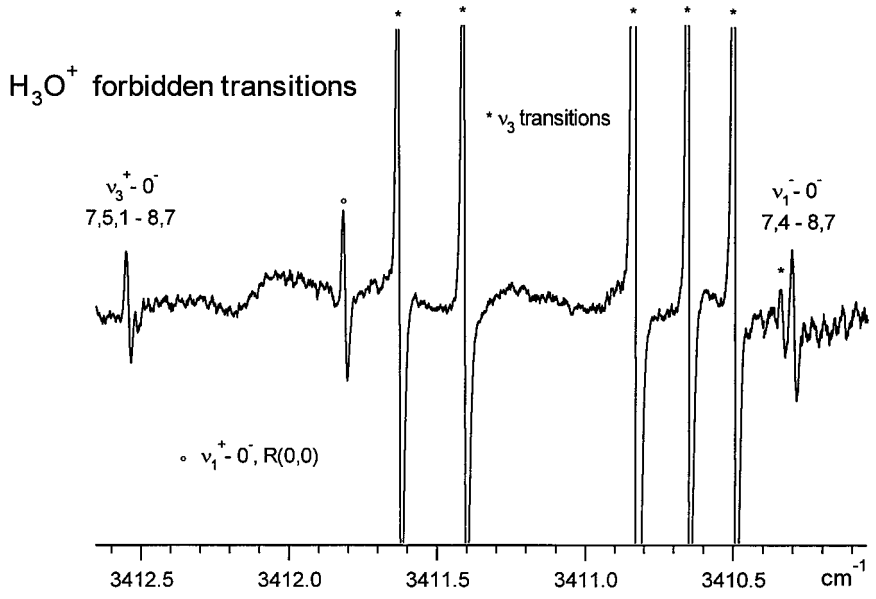

FIG. 3. Two observed forbidden transitions 7, 5, 1, $\nu_3^+ \leftarrow 8, 7, 0^-$ and 7, 4, $\nu_1^- \leftarrow 8, 7, 0^-$, which borrow intensity from the strongly allowed 7, 6, -1, $\nu_3^- \leftarrow 8, 7, 0^-$ transition due to upper level mixing. The strong lines with $*$ are the $\nu_3^\pm \leftarrow 0^\pm$ transitions (from the left) $^pP(6, 2)^+$, $^pP(9, 8)^+$, $^pP(8, 6)^+$, $^pP(5, 1)^-$, $^pP(7, 4)^+$, and $^rQ(11, 9)^-$.

ously observed (*17*) in the He-dominant discharges. Many spectral lines, such as those corresponding to H_2O^+, OH^+, and impurity ions NH_3^+ and NH_4^+, disappeared; also the lines corresponding to hot bands or higher J, K transitions of H_3O^+ became much weaker, reflecting the low temperature of the plasmas. The simplicity of this spectrum has made it easier to assign the remaining strong transitions of the ν_3 fundamental band and to look for the weak lines of the ν_1 fundamental band of H_3O^+.

III. SPECTRAL ASSIGNMENT

a. ν_3 Fundamental Band

The previous study (*5*) reported on the ν_3 fundamental band of H_3O^+-assigned transitions with rotational quantum numbers up to $J = K = 12$. However, many transitions with considerable intensities were left unassigned. For example, the transitions of $\nu_3^+ \leftarrow 0^+$ with $\Delta K = \Delta l = 1$ for $K'' \geq 4$ and the transitions of $\nu_3^\pm \leftarrow 0^\pm$ with $\Delta K = \Delta l = -1$ for $J'' > K'' \geq 7$ were missing in the previous line list (*5*).

In Table 1, we list 170 newly assigned transitions for the ν_3 fundamental band. We were able to assign these transitions based on their ground state combination differences, intensities, and calculated frequencies, although the observed frequencies were generally quite different from the calculated frequencies. Some transitions could not be confirmed by their ground state combination differences because the partner transitions fell into the strong water absorption regions. However, the sparse line distribution in the present spectrum made the assignment of strong transitions unambiguous.

TABLE 3

Observed Forbidden Transitions and Ground State Combination Differences for H_3O^+ (in cm^{-1})

Forbidden transitions								Allowed transitions								Combination differences							
J'	K'	l'		J	K		Obs.	J'	K'	l'		J	K		Obs.	J'	K'		J	K		Dif.	O-C
7	4	1	ν_3^+	8	6	0^-	3393.586	7	4	1	ν_3^+	8	3	0^+	3310.201	8	3	0^+	8	6	0^-	83.385	0.015
8	4	1	ν_3^+	9	6	0^-	3370.896	8	4	1	ν_3^+	9	3	0^+	3285.597	9	3	0^+	9	6	0^-	85.299	-0.015
6	5	1	ν_3^+	7	7	0^-	3433.494	6	5	1	ν_3^+	7	4	0^+	3324.687	7	4	0^+	7	7	0^-	108.807	-0.002
7	5	1	ν_3^+	8	7	0^-	3412.520	7	5	1	ν_3^+	8	4	0^+	3301.908	8	4	0^+	8	7	0^-	110.612	-0.006
7	4		ν_1^-	8	7	0^-	3410.298	7	4		ν_1^-	8	4	0^+	3299.684	8	4	0^+	8	7	0^-	110.614	-0.004
6	6	-1	ν_3^+	5	4	0^-	3518.542	6	6	-1	ν_3^+	7	7	0^+	3448.476	7	7	0^+	5	4	0^-	70.066	0.020
6	4		ν_1^+	7	7	0^+	3450.976	6	4		ν_1^+	7	4	0^-	3235.114	7	4	0^-	7	7	0^+	215.862	-0.041[a]
7	4		ν_1^+	7	7	0^+	3604.909[b]	7	4		ν_1^+	7	4	0^-	3388.970	7	4	0^-	7	7	0^+	215.939	0.036[a]
7	4		ν_1^+	8	7	0^+	3425.414	7	4		ν_1^+	8	4	0^-	3213.669[b]	8	4	0^-	8	7	0^+	211.745	0.026

[a] Not used in the fitting.

[b] Overlapped lines.

TABLE 4
Determined Molecular Constants of H_3O^+ (in cm^{-1} and with 1σ errors)

		$0^-\leftarrow 0^+$	$\nu_1^+\leftarrow 0^-$	$\nu_1^-\leftarrow 0^+$	$\nu_3^+\leftarrow 0^+$	$\nu_3^-\leftarrow 0^-$
ν_0		55.34840 (71)	3389.6561 (16)	3491.1696 (17)	3536.0364 (25)	3519.4370 (18)
			$v = 0$	ν_1		ν_3
B_v	(+)		11.25374 (11)	11.08146 (16)		11.02498 (14)
	(−)		11.05442 (11)	10.90655 (21)		10.87598 (10)
C_v	(+)		6.12906 (85)	6.07806 (17)		6.11886 (24)
	(−)		6.21131 (84)	6.14939 (11)		6.18462 (9)
$D_J^v \times 10^4$	(+)		13.062 (14)	13.599 (29)		11.827 (14)
	(−)		9.957 (15)	10.317 (51)		9.183 (11)
$D_{JK}^v \times 10^4$	(+)		-26.850 (37)	-28.167 (66)		-26.94 (10)
	(−)		-18.309 (36)	-16.629 (105)		-17.883 (30)
$D_K^v \times 10^4$	(+)		12.43 (12)	13.235 (58)		13.89 (12)
	(−)		6.64 (13)	4.334 (75)		7.109 (25)
ζ_3	(+)					0.077456 (86)
	(−)					0.078679 (46)
$\eta_J \times 10^4$	(+)					-10.06 (22)
	(−)					-11.57 (19)
$\eta_K \times 10^4$	(+)					-1.05 (44)
	(−)					-0.52 (17)
q	(+)					0.05962 (27) [b]
	(−)					0.05487 (9) [b]
$\beta \times 10^4$	(+)					1.678 (10) [b]
	(−)					1.949 (29) [b]

[a] Molecular constants for the ground state were determined by the least-squares fitting for sets of the $0^\pm$ data from Ref. (5), Ref. (19), and the $\Delta K = \pm 3$ combination differences in Table 3. Molecular constants for the ν_1 and ν_3 vibrations were determined by the least-squares fittings of the ν_1 and ν_3 fundamental bands with the molecular constants of the ground state fixed.

[b] The sign of q is different from the one in Ref. (5) and the value of β is twice of the one in Ref. (5) because of the different definitions (see Eq. [2] of Sec. IV).

Compared with the previously assigned transitions of lower J, K quantum numbers (5), the newly assigned transitions of $\nu_3^\pm \leftarrow 0^\pm$ showed much larger residuals between observation and calculation (see Table 1 and Sec. IV). These large residuals were the main reason why these transitions could not be assigned before.

b. ν_1 Fundamental Band

Having assigned all the strong transitions for the ν_3 fundamental band, we noticed two dense spectral features around 3389 (shown in Fig. 1) and 3490 cm^{-1} (shown in Fig. 2) that remained unassigned. Their typical patterns as Q-branch lines of parallel vibration–rotation bands made them candidates for the two Q branches of the $\nu_1^+ \leftarrow 0^-$ and $\nu_1^- \leftarrow 0^+$ bands of H_3O^+.

The Q branch spectral pattern of a parallel band depends on the differences of rotational constants between the upper and lower vibrational states, which should be quite different for the $\nu_1^+ \leftarrow 0^-$ and $\nu_1^- \leftarrow 0^+$ bands of H_3O^+. Assuming that B_v and $C_v - B_v$ for the ν_1 vibration are about average for the ground and the ν_3 states, which holds approximately in NH_3, we estimated the differences of B_v and $C_v - B_v$ between the $\nu_1^\pm$ and $0^\mp$ states. This gave us an idea about the two different Q-branch patterns for H_3O^+. Together with the expected intensity patterns, especially the doubled intensities for the $K = 0, 3, 6, \cdots$ spectral lines due to spin statistical weights, the two Q branches were assigned as shown in Fig. 1 and 2. The final assignment for the Q, P, and R branches of $\nu_1^\pm \leftarrow 0^\mp$ was confirmed by the ground state combination differences and are listed in Table 2.

c. Forbidden Transitions

In calculating the rovibrational energy in the ν_1 and ν_3 states, we found that some levels that are connected by vibration–rotation interactions are very close in energy ($\sim$1 cm^{-1}). Intensity borrowing resulting from the mixing of these near-resonance levels make forbidden transitions observable. For example, three energy levels (7, 6, -1, ν_3^-), (7, 5, 1, ν_3^+), and (7, 4, ν_1^-) are accidentally close. Vibration–rotation interactions (discussed later in Sec. V) make the forbidden transitions 7, 5, 1, $\nu_3^+ \leftarrow$ 8, 7, 0$^-$ and 7, 4, $\nu_1^- \leftarrow$ 8, 7, 0$^-$ clearly observable, as shown in Fig. 3, by intensity borrowing from the strongly allowed 7, 6, -1, $\nu_3^- \leftarrow$ 8, 7, 0$^-$ transition. Frequency of the forbidden transition was predicted by taking the difference between the observed frequency for an allowed transition and the calculated combination difference in the ground state with $\Delta K = \pm 3$ between 0$^+$ and 0$^-$. For example, the frequency of the forbidden transition 7, 5, 1, $\nu_3^+ \leftarrow$ 8, 7, 0$^-$ was calculated from the observed frequency for 7, 5, 1, $\nu_3^+ \leftarrow$ 8, 4, 0$^+$ and the calculated combination difference between 8, 7, 0$^-$ and 8, 4, 0$^+$. Therefore, the discrepancy between the predicted and observed frequencies for the forbidden transition revealed inaccurate calculations for the ground state levels, which in turn allowed us to determine the molecular constants C and D_K accurately (see Sec. IV). Altogether, nine forbidden transitions have been found as listed in Table 3.

IV. ANALYSIS

For the ground state and the nondegenerate ν_1 state of H_3O^+, a standard expression of vibration–rotation energy has been used

$$F_v(J, K) = \nu_0 + B_v J(J+1) + (C_v - B_v)K^2 - D_J^v J^2(J+1)^2 - D_{JK}^v J(J+1)K^2 - D_K^v K^4, \quad [1]$$

where ν_0 is a vibrational band origin, B_v and C_v are rotational constants, and D is the quartic centrifugal distortion constant.

For the doubly degenerate ν_3 state of H_3O^+, the diagonal vibration–rotation energy is (*5*)

$$F_v^l(J, K) = F_v(J, K) - [2\zeta_3 C_v - \eta_J J(J+1) - \eta_K K^2] \times Kl + (-1)^{\pi+J+1}[\delta_{k,1}\delta_{l,1}qJ(J+1) + \delta_{k,2}\delta_{l,-1}\beta(J-1)J(J+1)(J+2)]/2, \quad [2]$$

where l is the quantum number of the vibrational angular momentum, ζ_3 is the first-order Coriolis constant, η_J and η_K are the centrifugal distortion corrections of the Coriolis term, q and β are the A_1–A_2 splitting constants (the signs are different from Ref. (*5*), but are consistent with the conventional definition (*39*)), and $(-1)^\pi = \pm 1$ ($\pi = 0$ and 1) represents parity of the inversion state. Because the spatial wavefunction with A_1' or A_1'' symmetry is not allowed

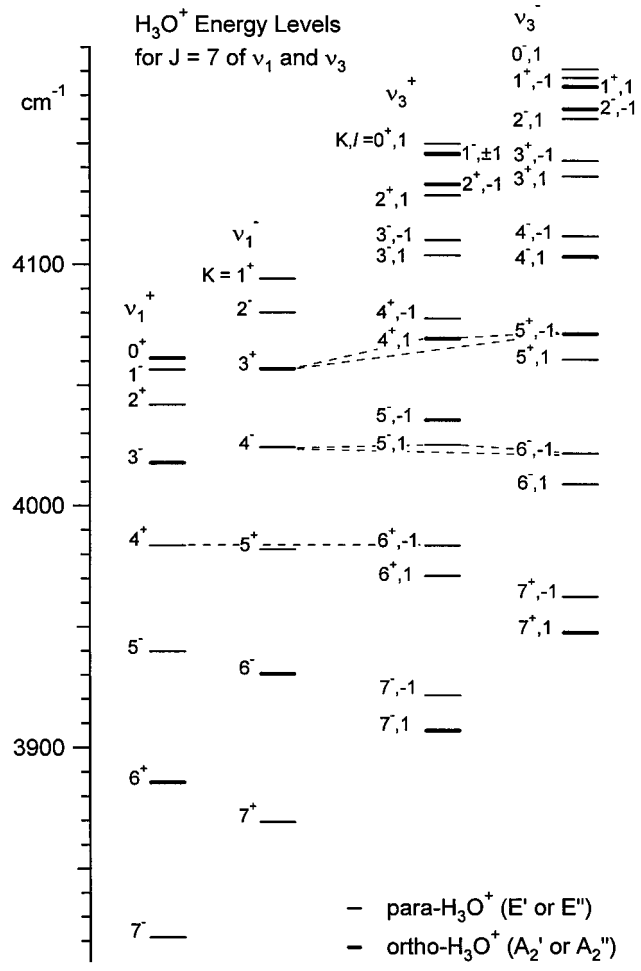

FIG. 4. Energy level diagram for $J = 7$ of the $\nu_1^\pm$ and $\nu_3^\pm$ states. The parity $(-1)^{k+\pi}$ for each level is indicated by a superscript of quantum number K. *Para* levels are drawn with thin lines and *ortho* levels with doubled spin statistical weights are drawn with bold lines. There are no vibration–rotation interactions between levels with different parities and between *ortho* and *para* levels. The $K = 4$ (ν_1^+) and $K = 6$ (ν_3^+, $l = -1$) levels interact strongly with each other through h_4 (Eqs. [7] and [11]) because of the small energy difference (0.65 cm^{-1}), and repelling shifts of 0.79 cm^{-1} were observed. The $K = 4$ (ν_1^-), $K = 5$ (ν_3^+, $l = 1$), and $K = 6$ (ν_3^-, $l = -1$) levels with small energy differences have cyclic interactions through h_3, h_2, and h_4, which result in a small shift of the middle level $K = 4$, a large upward shift of 1.26 cm^{-1} for $K = 5$, and a large downward shift of 1.15 cm^{-1} for $K = 6$.

to combine with the spin wavefunction of the A_1' symmetry (the Pauli principle), only one component of the A_1–A_2 split levels, that is, the A_2' or A_2'' symmetry level constructed from the $k = l = \pm 1$ combination or the $k = \pm 2$, $l = \mp 1$ combination, is present with a staggering shift as shown in the last two terms of Eq. [2]. The interaction term

$$h_1 = q(q_{3+}^2 J_-^2 + q_{3-}^2 J_+^2)/4, \quad [3]$$

which causes the l-type doubling in Eq. [2] for otherwise

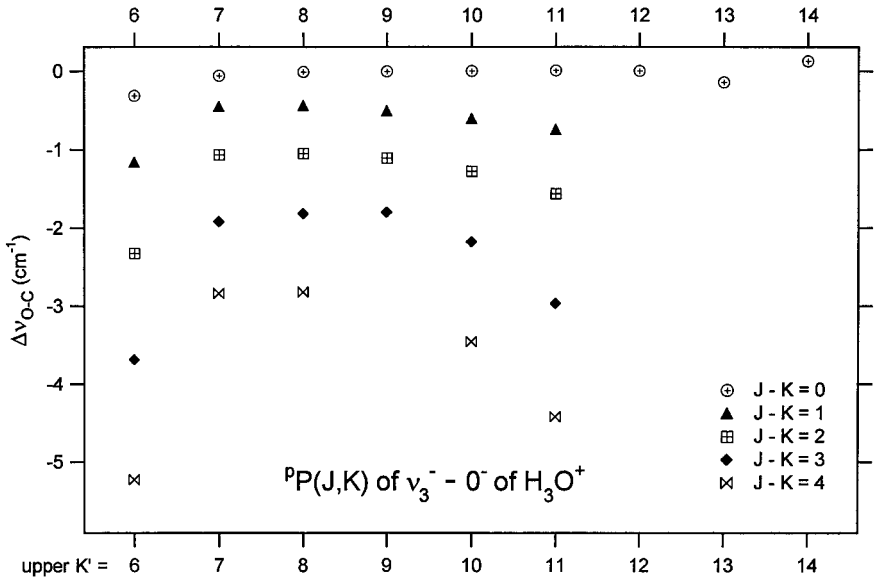

FIG. 5. A diagram showing deviations $\Delta\nu_{o-c}$ between observed and calculated frequencies as functions of K' and $J - K$ for the ${}^pP(J, K)$ transitions of the $\nu_3^- \leftarrow 0^-$ band. It is noted that $\Delta\nu_{o-c}$ increases linearly with $J - K$ for certain K'. $\Delta\nu_{o-c}$ for $K' = 6$ is abnormally large because of the strong interaction with the $K' = 4$ levels of ν_1^-.

degenerate $k = l = \pm 1$ levels, causes also l-type resonance by its off-diagonal element

$$\langle \nu_3^{\pm},\, l = 1,\, J,\, K + 1 | h_1 | \nu_3^{\pm},\, l = -1,\, J,\, K - 1 \rangle = q\{[J(J + 1) - K(K - 1)] \times [J(J + 1) - K(K + 1)]\}^{1/2}/2, \quad [4]$$

where $q = q_0 + q_J J(J + 1) + q_K K^2$.

As mentioned in Section IIIc, observation of forbidden transitions has enabled us to determine energy differences with $\Delta K = 3$ in the ground state. In the previous study on forbidden transitions (*6*), an energy difference between $K = 0$ of the inversion 0^+ state and $K = 3$ of the 0^- state was obtained, which led to a determination of the rotational C'' constant of the ground state by fixing D_K at the theoretical value (*33*). In the present study, additional energy differences between $K = 3$, 0^+ and 6, 0^- and between $K = 4$, $0^{\pm}$ and 7, $0^{\mp}$, which have

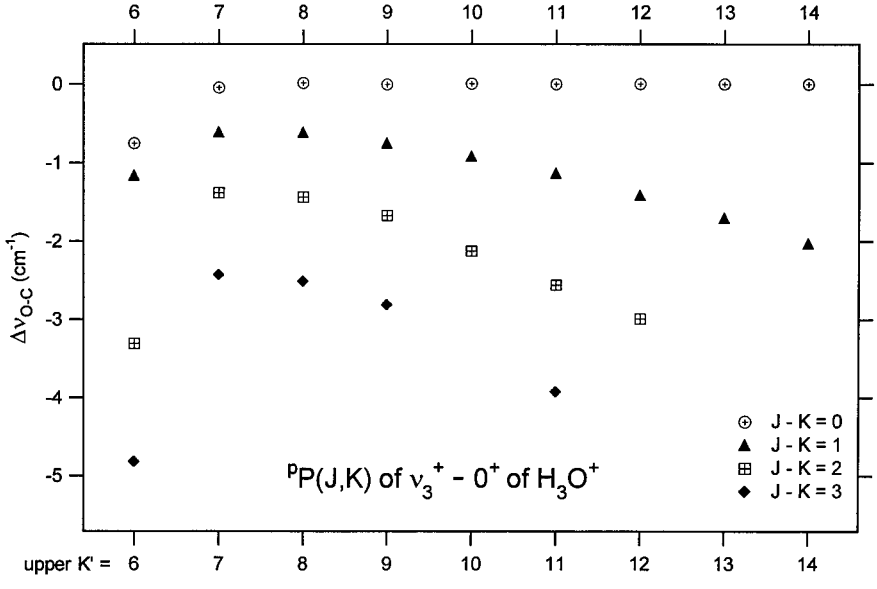

FIG. 6. A diagram showing deviations $\Delta\nu_{o-c}$ between observed and calculated frequencies as functions of K' and $J - K$ for the ${}^pP(J, K)$ transitions of the $\nu_3^+ \leftarrow 0^+$ band. It is noted that $\Delta\nu_{o-c}$ increases linearly with $J - K$ for certain K'. $\Delta\nu_{o-c}$ for $K' = 6$ is abnormally large because of the strong interaction with the $K' = 4$ levels of ν_1^+.

TABLE 5
Rotational Constants, Inertia Defects, and Equilibrium Structure of H_3O^+

		B_v (cm^{-1})	C_v (cm^{-1})	Δ_v (amu·Å^2)
$v = 0$	(+)	11.25374 (11)	6.12906 (85)	-0.2455
	(−)	11.05442 (11)	6.21131 (84)	-0.3359
ν_1	(+)	11.08146 (16)	6.07806 (17)	-0.2690
	(−)	10.90655 (21)	6.14939 (11)	-0.3499
ν_2 [a]	(+)	11.18247 (14)	6.0871 (12)	-0.2456
	(−)	10.69741 (12)	6.2590 (12)	-0.4584
ν_3	(+)	11.02497 (14)	6.11887 (24)	-0.3031
	(−)	10.87591 (9)	6.18464 (9)	-0.3743
ν_4 [b]	(+)	11.5840 (16)	6.0468 (21)	-0.1226
	(−)	11.3481 (22)	6.1418 (27)	-0.2263
		B_e (cm^{-1})	C_e (cm^{-1})	Δ_e (amu·Å^2)
Present [c]	(+)	11.2740 (23)	6.2680 (64)	-0.3010
	(−)	11.1917 (29)	6.3146 (68)	-0.3429
	average	11.2329 (26)	6.2913 (66)	-0.3220
ab initio [d]		11.082	6.415	-0.4146
		r_e (Å)	α_e (∠HOH, deg.)	
Present [c]	(+)	0.9740 (9)	113.98 (7)	
	(−)	0.9749 (9)	113.18 (7)	
	average	0.9744 (9)	113.58 (7)	
ab initio	Ref. (31)	0.975	111.82	
	Ref. (32)	0.9745	111.88	
	Ref. (33)	0.975	111.7	

[a] Molecular constants from Ref. (14).

[b] Molecular constants from Ref. (15).

[c] Equilibrium values in (+) and (–) are derived from the above sets of molecular constants for the + and – inversion states, respectively.

[d] Calculated from the structural parameters of Ref. (33).

much higher centrifugal distortion correction, have allowed us to determine accurate values of both C'' and D''_K of the ground state. Seven combination differences obtained from the forbidden transitions given in Table 3 were used in the fitting. Together with the far-infrared data of the $0^- \leftarrow 0^+$ transitions in Ref. (*19*) and the ground state combination differences in Ref. (*5*), these $\Delta K = 3$ combination differences were least-squares fitted to determine a set of molecular constants in the ground $0^\pm$ state. In the least-squares fitting, five times the larger weight was put on the far-infrared data for their higher accuracy. The determined ground state constants are shown in Table 4. They should provide accurate prediction for the rotation–inversion spectrum of interstellar H_3O^+.

For the determination of molecular constants in the excited states, each subband of $\nu_1^\mp \leftarrow 0^\pm$ and $\nu_3^\pm \leftarrow 0^\pm$ was least-squares fitted individually with the vibration–rotation expressions of Eqs. [1–4]. The ground state constants were fixed at the values determined in the above analysis.

Thirty-three transitions of the $\nu_1^- \leftarrow 0^+$ band and 51 transitions of the $\nu_1^+ \leftarrow 0^-$ band in Table 2 were included in the least-squares analysis. The determined molecular constants for $\nu_1^\pm$ are shown in Table 4. Transitions with upper quantum number $J' \leq 4$ were all fit with residuals less than or comparable to the experimental accuracy for frequency measurement (typically 0.006 cm^{-1}). For $J' \geq 5$, most transitions with $J' = K'$ were fit well, but many transitions with $J' > K'$ deviated significantly from the calculated frequencies, as shown in Table 2, among which the largest discrepancy reached to 0.8 cm^{-1}. These large deviations are discussed later.

None of the newly assigned lines for the $\nu_3^\pm \leftarrow 0^\pm$ transitions could be included in the least-squares fitting because of their large deviations. Therefore, not much improvement on fitting

of the molecular constants of the ν_3 state was made over the results of Ref. (5). However, our determination of C'' and D''_K in the ground state has allowed us to give molecular constants individually as shown in Table 4.

V. DISCUSSION

Besides the off-diagonal Coriolis interaction of Eq. [3] that links the $\Delta k = \Delta l = \pm 2$ levels within ν_3^+ or ν_3^-, there are three other sizable off-diagonal vibration–rotation operators (*39–42*) for a C_{3v} molecule:

$$h_2 = r_t[(q_{3+}^2 J_+ + q_{3-}^2 J_-)J_z + J_z(q_{3+}^2 J_+ + q_{3-}^2 J_-)], \quad [5]$$

$$h_3 = B\zeta_{13}[(q_{3+}J_- + q_{3-}J_+)p_1\sqrt{\nu_1/\nu_3} - (p_{3+}J_- + p_{3-}J_+)q_1\sqrt{\nu_3/\nu_1}], \quad [6]$$

and

$$h_4 = -\alpha_{13}[(q_{3+}J_+^2 + q_{3-}J_-^2)q_1 + (p_{3+}J_+^2 + p_{3-}J_-^2)p_1]/2, \quad [7]$$

where the ladder operators are $a_\pm = a_x \pm a_y$, and r_t, ζ_{13}, and a_{13} are vibration–rotation interaction parameters. These operators link levels between ν_3^+ and ν_3^- or between ν_1 and ν_3 but have not been considered explicitly in our least-squares analysis of Section IV. The operator of Eq. [5] links levels of the ν_3^+ and ν_3^- states by the matrix element

$$\langle \nu_3^\pm, l = 1, J, K|h_2|\nu_3^\mp, l = -1, J, K+1\rangle = 2r_t(2K+1)[J(J+1) - K(K+1)]^{1/2}, \quad [8]$$

which is sometimes called the "2, −1" *l*-type interaction (*39*). The operator of Eq. [6], the Coriolis interaction, links levels of the $\nu_1^\pm$ and $\nu_3^\mp$ states by the matrix elements

$$\langle \nu_1^\pm, J, K|h_3|\nu_3^\mp, l = 1, J, K+1\rangle = iw_{13}[J(J+1) - K(K+1)]^{1/2}, \quad [9]$$

$$\langle \nu_1^\pm, J, K|h_3|\nu_3^\mp, l = -1, J, K-1\rangle = iw_{13}[J(J+1) - K(K-1)]^{1/2}, \quad [10]$$

where $w_{13} = B\,\zeta_{13}\,(\nu_1 + \nu_3)/\sqrt{2\nu_1\nu_3}$. The operator of Eq. [7], the Birss interaction (*41, 42*), links levels of the $\nu_1^\pm$ and $\nu_3^\pm$ states by the matrix elements

$$\begin{aligned}\langle \nu_1^\pm, J, K+1|h_4|\nu_3^\pm, l = 1, J, K-1\rangle &= \langle \nu_1^\pm, J, K-1|h_4|\nu_3^\pm, l = -1, J, K+1\rangle \\ &= -a_{13}\{[J(J+1) - K(K-1)] \\ &\quad \times [J(J+1) - K(K+1)]\}^{1/2}/\sqrt{2}.\end{aligned} \quad [11]$$

The phase factors are chosen such that matrix elements of q_1, $q_{3\pm}$, and $J_\pm$ are real and those of p_1 and $p_{3\pm}$ are imaginary.

All the interactions are between levels with same J, parity, and spin modification (*ortho* or *para*), i.e., with $\Delta J = 0$, $\Delta(k + \pi) = 0$ (mod. 2), and $\Delta(k - l) = 0$ (mod. 3). An example of the mixing for the energy levels with $J = 7$ of $\nu_1^\pm$ and $\nu_3^\pm$ is illustrated in Fig. 4. The ($\nu_1^\pm$, J, K) and ($\nu_3^\pm$, $l = -1$, J, $K + 2$) levels, linked by the h_4 interaction, are close and the order reverses between $K = 3$ and $K = 4$. The energy differences between $K = 4$ (ν_1^+) and $K = 6$ (ν_3^+, $l = -1$) without considering the h_4 interaction are only 0.91 cm^{-1} for $J = 6$ and 0.65 cm^{-1} for $J = 7$. The large residuals $\Delta\nu_{o-c}$ for the $\nu_1^+ \leftarrow 0^-$ transitions involving $J' \geq K' + 2$ ($K' = 3$, 4, and 5) are reduced by taking into account the h_4 interaction with $a_{13} \approx 0.08$ cm^{-1}. The level mixing by the h_4 interaction also induces the forbidden transition as discussed in Section IIIc.

The mixing between the (ν_1^-, J, K) and (ν_3^-, $l = -1$, J, $K + 2$) levels is complicated by the participation of another level (ν_3^+, $l = 1$, J, $K + 1$). The interactions h_4, h_3, and h_2 each connect two of the three levels. For $J = K$, the interactions do not exist and the ν_1 transitions fit well. When $J = K + 1$, the (ν_3^-, $l = -1$, J, $K + 2$) level does not exist and the only interaction is h_3 between (ν_1^-, J, K) and (ν_3^+, $l = 1$, J, $K + 1$). To explain the residuals $\Delta\nu_{o-c}$ for the $\nu_1^- \leftarrow 0^+$ transitions involving the (ν_1^-, 5, 4) and (ν_1^-, 6, 5) levels, $w_{13} \approx 0.22$ cm^{-1} and 0.35 are required, respectively. For $K = 4$ and $J = 6$ or 7, three nearly resonant levels exist and we have to consider the three interactions simultaneously. Although it is impossible to get a unique solution for the three parameters from two independent $\Delta\nu_{o-c}$, a set of values $r_t \approx 0.01$ cm^{-1}, $w_{13} \approx 0.2$ cm^{-1}, and $a_{13} \approx 0.07$ cm^{-1} are the reasonable solutions for both $J = 6$ and $J = 7$. The values for w_{13} and a_{13} are comparable with the ones determined above from other interacting levels. From $w_{13} \approx 0.2$ cm^{-1}, ζ_{13} is calculated to be 0.013, which is similar to the value 0.017 in NH_3 (*43*).

Although most of the large residuals for the $\nu_1^\pm \leftarrow 0^\mp$ transitions were explained by the h_2, h_3, and h_4 interactions, it was not straightforward to understand the even larger residuals for the $\nu_3^\pm \leftarrow 0^\pm$ transitions. In Figs. 5 and 6, we plotted the residuals for the newly assigned ^pP transitions ($K' \geq 6$) of $\nu_3^\pm \leftarrow 0^\pm$, which gives deviations of the upper levels. The large and irregular $\Delta\nu_{o-c}$ for $K' = 6$ can be ascribed mainly to the h_4 interactions between the ($\nu_1^\pm$, J, $K = 4$) and ($\nu_3^\pm$, $l = -1$, J, $K = 6$) levels discussed above. For $K' \geq 7$, there is a regular variation for the residuals, that is, $\Delta\nu_{o-c}$ rises proportionally to J–K, which appears for the square of the h_2 or h_3 matrix elements in Eqs. [8–10]. However, the K-dependent feature for a certain J–K does not correspond to these squared matrix elements.

Because the B and C rotational constants of all the fundamental vibrations are now available for H_3O^+, equilibrium rotational constants and equilibrium structure of H_3O^+ could be derived, as shown in Table 5. The obtained bond length is in good agreement with the theoretical value, but the angle

$\angle$HOH is about 1.7° larger than the *ab initio* value, which means that theoretical calculations give more nonplanar structure. For a nearly planar molecule, the inertial defect, $\Delta = I_{cc} - 2I_{bb}$, gives a good measure for planarity of a molecular structure (*44*). The theoretical structure gives $\Delta = -0.4146$ a.m.u. Å^2, while our experimental value is $\Delta = -0.3299$ a.m.u. Å^2. In fact, observed inertial defects (see Table 5) for the ground and fundamental vibrational states of H_3O^+ are all between -0.13 and -0.38, except for -0.4655 of ν_2^-, which is due to the large out-of-plane inversion motion.

ACKNOWLEDGMENTS

This work was supported by the NSF Grant PHY-9722691.

REFERENCES

1. M. H. Begemann, C. S. Gudeman, J. Pfaff, and R. J. Saykally, *Phys. Rev. Lett.* **51,** 554–557 (1983).
2. P. R. Bunker, T. Amano, and V. Špirko, *J. Mol. Spectrosc.* **107,** 208–211 (1984).
3. M. H. Begemann and R. J. Saykally, *J. Chem. Phys.* **82,** 3570–3579 (1985). [See also E. R. Keim, M. L. Polak, J. C. Owrutsky, J. V. Coe, and R. J. Saykally, *J. Chem. Phys.* **93,** 3111 (1990).]
4. A. Stahn, H. Solka, H. Adams, and W. Urban, *Mol. Phys.* **60,** 121–128 (1987).
5. W. C. Ho, C. J. Pursell, and T. Oka, *J. Mol. Spectrosc.* **149,** 530–541 (1991).
6. D. Uy, E. T. White, and T. Oka, *J. Mol. Spectrosc.* **183,** 240–244 (1997).
7. N. N. Haese and T. Oka, *J. Chem. Phys.* **80,** 572–573 (1984).
8. B. Lemoine and J. L. Destombes, *Chem. Phys. Lett.* **111,** 284–287 (1984).
9. P. B. Davies, P. A. Hamilton, and S. A. Johnson, *Astron. Astrophys.* **141,** L9–L10 (1984).
10. P. B. Davies, P. A. Hamilton, and S. A. Johnson, *J. Opt. Soc. Am.* B**2,** 794–799 (1985).
11. D.-J. Liu, N. N. Haese, and T. Oka, *J. Chem. Phys.* **82,** 5368–5372 (1985).
12. D.-J. Liu and T. Oka, *Phys. Rev. Lett.* **54,** 1787–1789 (1985).
13. P. B. Davies, S. A. Johnson, P. A. Hamilton, and T. J. Sears, *Chem. Phys.* **108,** 335–341 (1986).
14. D.-J. Liu, T. Oka, and T. J. Sears, *J. Chem. Phys.* **84,** 1312–1316 (1986).
15. M. Gruebele, M. Polak, and R. J. Saykally, *J. Chem. Phys.* **87,** 3347–3351 (1987).
16. M. Bogey, C. Demuynck, M. Denis, and J. L. Destombes, *Astron. Astrophys.* **148,** L11–L13 (1985).
17. G. M. Plummer, E. Herbst, and F. C. DeLucia, *J. Chem. Phys.* **83,** 1428–1429 (1985).
18. P. Verhoeve, J. J. ter Meulen, W. Leo Meerts, and A. Dymanus, *Chem. Phys. Lett.* **143,** 501–504 (1988).
19. P. Verhoeve, M. Versluis, J. J. ter Meulen, W. Leo Meerts, and A. Dymanus, *Chem. Phys. Lett.* **161,** 195–201 (1989).
20. J. M. Hollis, E. B. Churchwell, E. Herbst, and F. C. DeLucia, *Nature* **322,** 524–526 (1986).
21. A. Wootten, F. Boulanger, M. Bogey, F. Combes, P. J. Encrenaz, M. Gerin, and L. Ziurys, *Astron. Astrophys.* **166,** L15–L18 (1986).
22. A. Wootten, J. G. Mangum, B. E. Turner, M. Bogey, F. Boulanger, F. Combes, P. J. Encrenaz, and M. Gerin, *Astrophys. J.* **380,** L79–L83 (1991).
23. T. G. Phillips, E. F. van Dishoeck, and J. Keene, *Astrophys. J.* **399,** 533–550 (1992).
24. R. Timmermann, T. Nikola, A. Poglitsch, N. Geis, G. J. Stacey, and C. H. Townes, *Astrophys. J.* **463,** L109–L112 (1996).
25. P. A. Giguère and C. Madec, *Chem. Phys. Lett.* **37,** 569–573 (1976).
26. G. H. F. Diercksen, W. P. Kraemer, and B. O. Roos, *Theor. Chim. Acta.* **36,** 249–274 (1975).
27. V. Špirko and P. R. Bunker, *J. Mol. Spectrosc.* **95,** 226–235 (1982).
28. P. R. Bunker, W. P. Kraemer, and V. Špirko, *J. Mol. Spectrosc.* **101,** 180–185 (1983).
29. M. E. Colvin, G. P. Raine, H. F. Schaefer III, and M. Dupuis, *J. Chem. Phys.* **79,** 1551–1552 (1983).
30. P. Botschwina, P. Rosmus, and E.-A. Reinsch, *Chem. Phys. Lett.* **102,** 299–306 (1983).
31. N. Shida, K. Tanaka, and K. Ohno, *Chem. Phys. Lett.* **104,** 575–578 (1984).
32. P. Botschwina, *J. Chem. Phys.* **84,** 6523–6524 (1986).
33. V. Špirko and W. P. Kraemer, *J. Mol. Spectrosc.* **134,** 72–81 (1989).
34. E. P. F. Lee and J. M. Dyke, *Mol. Phys.* **73,** 375–405 (1991).
35. F. DiGiacomo, F. A. Gianturco, F. Raganelli, and F. Schneider, *J. Chem. Phys.* **101,** 3952–3961 (1994).
36. M. W. Crofton, M.-F. Jagod, B. D. Rehfuss, W. A. Kreiner, and T. Oka, *J. Chem. Phys.* **88,** 666–678 (1988).
37. M. G. Bawendi, B. D. Rehfuss, and T. Oka, *J. Chem. Phys.* **93,** 6200–6209 (1990).
38. C. S. Gudeman, M. H. Begemann, J. Pfaff, and R. J. Saykally, *Phys. Rev. Lett.* **50,** 727–731 (1983).
39. G. J. Cartwright and I. M. Mills, *J. Mol. Spectrosc.* **34,** 415–439 (1970).
40. T. Oka, *J. Chem. Phys.* **47,** 5410–5426 (1967).
41. F. W. Birss, *Mol. Phys.* **31,** 491–500 (1976).
42. W. A. Majewski, M. D. Marshall, A. R. W. McKellar, J. W. C. Johns, and J. K. G. Watson, *J. Mol. Spectrosc.* **122,** 341–355 (1987).
43. W. S. Benedict, E. K. Plyler, and E. D. Tidwell, *J. Chem. Phys.* **32,** 32–44 (1960).
44. T. Oka and Y. Morino, *J. Mol. Spectrosc.* **6,** 472–482 (1961).